Available online at www.sciencedirect.com
SCIENCE DIRECT®
International Journal of Heat and Mass Transfer 47 (2004) 1863–1875
International Journal of HEAT and MASS TRANSFER
www.elsevier.com/locate/ijhmt

Direct contact condensation in Hiemenz flow boundary layers

J. Davis, G. Yadigaroglu *

Nuclear Engineering Laboratory, Swiss Federal Institute of Technology, ETH-Zentrum CLT, CH-8092 Zurich, Switzerland

Received 18 February 2003; received in revised form 6 October 2003

Abstract

Direct contact condensation in two adjacent Hiemenz stagnation-flow boundary layers is investigated numerically for the cases of saturated and superheated vapor on subcooled liquid. Resulting parametric studies provide detailed information on the importance of specific parameters and, more importantly, provide heat and mass transfer correlations.

1. Introduction

Problems involving direct contact condensation are of practical interest, as this mode of condensation can offer enhanced heat transfer rates as compared with filmwise or dropwise condensation. An example of direct contact condensation is shown in Fig. 1a, which depicts part of a safety system in a passive boiling water reactor. In the case of an accident, condensable vapor is injected into subcooled liquid from the vent (shown in the figure) at a velocity v_J to help depressurize the system. If the velocity of the liquid–vapor interface, v_I, is subtracted from the flowfield, we expect to find a flow as shown in Fig. 1b. Restricting the domain of interest to the stagnation region, and neglecting the curvature of the surface, we obtain a flow as shown in Fig. 1c. With the liquid–vapor interface separating the two phases, the problem can be decomposed into two separate stagnation flows. In the vapor phase, we have a stagnation flow with suction and similarly in the liquid we have a stagnation flow with blowing. The flows, however, are clearly coupled by the interfacial jump conditions discussed below. For each phase, we can obtain the flow and temperature fields from the steady, laminar Hiemenz stagnation boundary layer solution [1,2]. In practice, the flow in the reactor is both unsteady and turbulent. The present study, however, deals with a simpler, obtainable, solution to this problem and looks into fundamental aspects of laminar direct contact condensation.

The solution of coupled two-fluid boundary layer flows has been the subject of previous studies. Wang [3] studied a non-isothermal stagnation flow on the surface of a denser fluid in absence of mass transfer. He simplified the problem by setting the free stream velocity of the denser fluid equal to zero; for this case the solution of the momentum equation is known [4]. Gerner and Tien [5] presented an axi-symmetric condensation solution for two impinging stagnation jets over a flat interface (Homann boundary layer flow [2,6]) which took into account non-condensables. Results are limited to a discussion of a few cases with specific combinations of variables; no correlations are derived. Coward and Hall [7] studied an isothermal stagnation flow over a finite liquid layer with allowance for mass transfer between the lower wall boundary and the liquid layer. Boyadjiev and Halatchev [8] studied the linear stability of an isothermal gas layer flowing over a liquid layer (Blasius boundary layer flow [2,9]) with mass transfer through the interface; the concentration gradients in the liquid were taken as zero. Tilley and Weidman [10] studied solutions of two oblique isothermal stagnation point flows forming a flat interface, without mass transfer, however.

Another group of studies worth noting are those of film condensation, where a vapor condenses over a subcooled plate. This physically different situation has been successfully studied using similarity relations to

* Corresponding author. Tel.: +41-1-632-4615; fax: +41-1-632-1166.
E-mail address: yadi@ethz.ch (G. Yadigaroglu).

0017-9310/$ - see front matter © 2003 Elsevier Ltd. All rights reserved.
doi:10.1016/j.ijheatmasstransfer.2003.10.009

Nomenclature

a, b	constant coefficients
B_p	blowing parameter; $\frac{v_0}{u_\infty}Re^{1/2}$
c	constants in $u = cx(1/s)$
c_p	specific heat capacity (J/kg K)
h_{LV}	evaporation enthalpy; $h_V - h_L$ (J/kg)
He_0	Hiemenz number; $(P_{L,0} - P_{V,0})/\mu c$
Ja	Jacob number; $c_p(T_\infty - T_0)/h_{LV}$
$\dot{m}$	specific mass transfer rate (kg/m^2 s)
Nu	Nusselt number; $\alpha x/\lambda$
P	pressure (N/m^2)
Pr	Prandtl number; $c_p\mu/\lambda$
Re	Reynolds number; $\rho c x^2/\mu$
T	temperature (K)
u	tangential velocity (m/s)
v	normal velocity (m/s)
v_I	velocity of the interface in a stationary frame of reference (m/s)
v_J	velocity of steam exiting pipe in a stationary frame of reference (m/s)
y, x	normal and tangential coordinate position (m)

Greek symbols

α	heat transfer coefficient; $\lambda\frac{\partial T}{\partial y}\Big\|_0/(T_\infty - T_0)$ (W/m^2 K)
ζ	velocity similarity variable; $\Psi/\sqrt{\frac{\mu x u_\infty}{\rho}}$
η	position similarity variable; $y\sqrt{\frac{\rho u_\infty}{\mu x}}$
Θ	temperature similarity variable; $(T - T_0)/(T_\infty - T_0)$
λ	thermal conductivity (W/m K)
μ	dynamic viscosity (N s/m^2)
ρ	density (kg/m^3)
Ψ	stream function such that $u = \partial\Psi/\partial y$ and $v = -\partial\Psi/\partial x$ (m^2/s)
Φ	correction coefficient for superheat

Subscripts

0	coordinate location $y = 0$
∞	coordinate location $y = \infty$
i	phase; $i \in \{L, V\}$
j	coordinate location $j \in (x, y)$
L	liquid phase
sat	saturated
sup	superheated
V	vapor phase

account for various effects such as non-condensables [11], varying flow properties [12], and superheated vapor [13]. A review of film condensation can be found in [14].

A similar study to the present one was performed by Davis and Yadigaroglu [15] for the condensation of a saturated vapor on subcooled liquid with a curved interface (curvature a function of x). The authors determined a correlation for mass transfer; however, the study did not include the effects of vapor superheat or varying viscosity ratio. Moreover, in the previous paper a surface tension force was considered, which, due to the requirement of matching the pressure gradients at the interface resulted in a non-flat interfacial topology of varying curvature; this introduced the free-stream velocities as independent variables. In the present paper we solve the direct contact condensation problem for a flat interface (no surface tension force), for both saturated and superheated vapor and study the effects of the viscocity ratio on heat and mass transfer.

The remainder of the paper is broken up as follows. In Section 2, the conservation equations and boundary conditions for each phase are described. Section 3 then provides the coupling between phases by introducing the interfacial jump conditions. Next, the solution algorithm is discussed in Section 4 along with a simplified solution. Section 5 then discusses results for the case of saturated vapor on subcooled liquid. Finally, Section 6 discusses results for the case of superheated vapor on subcooled liquid.

2. Conservation equations

The Hiemenz boundary layer flow [1] is a two-dimensional, steady-state flow for which the conservation equations for mass, u- and v-momentum and energy, for each phase i, are:

$$\frac{\partial u_i}{\partial x_i} + \frac{\partial v_i}{\partial y_i} = 0 \tag{1}$$

$$\rho_i u_i \frac{\partial u_i}{\partial x_i} + \rho_i v_i \frac{\partial u_i}{\partial y_i} = \mu_i \frac{\partial^2 u_i}{\partial y_i^2} - \frac{\partial P_i}{\partial x_i} \tag{2}$$

$$\rho u_i \frac{\partial v_i}{\partial x_i} + \rho_i v_i \frac{\partial v_i}{\partial y_i} = \mu_i \frac{\partial^2 v_i}{\partial y_i^2} - \frac{\partial P_i}{\partial y_i} \tag{3}$$

$$c_{p,i}\rho_i u_i \frac{\partial T_i}{\partial x_i} + c_{p,i}\rho_i v_i \frac{\partial T_i}{\partial y_i} = \lambda_i \frac{\partial^2 T_i}{\partial y_i^2} \tag{4}$$

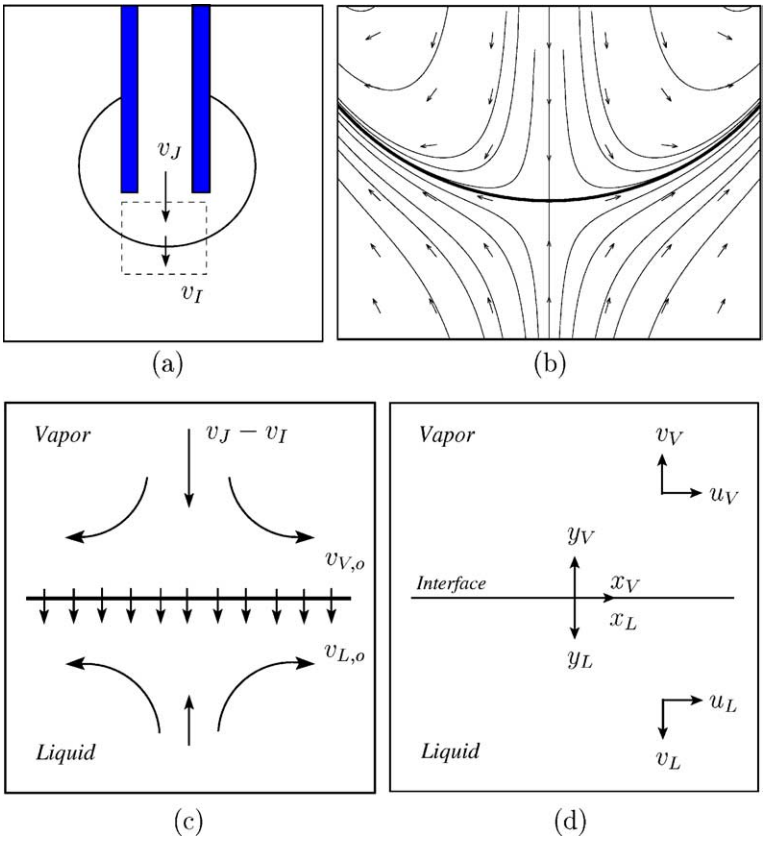

Fig. 1. (a) Injection of vapor in a stationary frame of reference. (b) View of dashed area in a frame of reference moving with velocity of the interface v_1. (c) Closeup of stagnation region. (d) Coordinate system setup.

with boundary conditions,

$$y_i \to \infty \begin{cases} u_i \to u_{i,\infty} \\ T_i \to T_{i,\infty} \end{cases}, \quad y_i = 0 \begin{cases} u_i = u_{i,0} \\ v_i = v_{i,0} \\ T_i = T_{i,0} = T_{\text{sat}} \end{cases} \tag{5}$$

where, at the freestream boundary ($y_i \to \infty$), the potential solution

$$u_i = c_i x_i, \quad v_i = -c_i y_i \tag{6}$$

$$P_i = P_{i,0} - \frac{1}{2}\rho_i c_i^2 \left(x_i^2 + y_i^2\right) \tag{7}$$

$$T_i = T_{i,0} + (T_{i,\infty} - T_{i,0})\text{erf}\left[\frac{\sqrt{2}}{2} Pr_i^{1/2} \left(\frac{\rho_i c_i}{\mu_i}\right)^{1/2} y_i\right] \tag{8}$$

is recovered. The coordinate system used is shown in 1d where the interface is taken at $y_V = y_L = 0$. Allowance for tangential movement of fluid at the boundary ($y_i = 0$) is provided using $u_{i,0} = c_{i,0} x_i$. Next, using the stream function, Ψ_i,

$$u_i = \frac{\partial \Psi_i}{\partial y_i}, \quad v_i = -\frac{\partial \Psi_i}{\partial x_i} \tag{9}$$

and similarity relations

$$\zeta_i(\eta_i) \equiv \Psi_i \sqrt{\frac{\rho_i}{\mu_i c_i x_i^2}}, \quad \eta_i \equiv y_i \sqrt{\frac{\rho_i c_i}{\mu_i}} \tag{10}$$

$$\Theta_i(\eta_i) \equiv \frac{T_i - T_{i,0}}{T_{i,\infty} - T_{i,0}} \tag{11}$$

the governing Eqs. (1)–(4) are transformed into a set of non-dimensional ordinary differential equations:

$$\zeta_i''' + \zeta_i \zeta_i'' - (\zeta_i')^2 + 1 = 0 \tag{12}$$

$$\Theta_i'' + Pr_i \zeta_i \Theta_i' = 0 \tag{13}$$

where the superscripts $'$, $''$, and $'''$ depict the derivatives $\frac{\partial^3}{\partial \eta^3}$, $\frac{\partial^2}{\partial \eta^2}$, and $\frac{\partial}{\partial \eta}$ respectively. Similarly, the boundary conditions (5) become

$$\eta_i \to \infty \begin{cases} \zeta_i' \to 1 \\ \Theta_i \to 1 \end{cases}, \quad \eta_i = 0 \begin{cases} \zeta_i = -B_{\text{p},i} \\ \zeta_i' = u_{i,0}/u_{i,\infty} \\ \Theta_i = 0 \end{cases} \tag{14}$$

where

$$B_{\mathrm{p},i} \equiv v_{i,0} c_i^{-1/2} \left(\frac{\rho_i}{\mu_i}\right)^{1/2} \tag{15}$$

Eqs. (12) and (13) with boundary conditions (14) describe the Hiemenz boundary layer flow. It is important to note that ζ and Θ in these equations depend only on η and are independent of x. The pressure distribution within the boundary layer, is given by

$$P_i = P_{i,0} + \mu_i c_i (1 - \zeta_i') - \frac{1}{2}\mu_i c_i \zeta_i^2 - \frac{1}{2}\rho_i c_i^2 x_i^2 \tag{16}$$

which upon differentiating with respect to x becomes

$$\left.\frac{\partial P}{\partial x}\right|_i = -\rho_i c_i^2 x_i \tag{17}$$

The complete derivation of these equations can be found in a number of texbooks (see for example Schlichting [2] or Kays and Crawford [16]) and is not repeated here.

3. Interfacial jump conditions

In addition to satisfying the conservation equations in the bulk of the liquid and vapor phases, one must assure that the interfacial jump conditions are met between phases. Starting with the interfacial jump conditions [17], and allowing no slip at the interface (i.e. $u_{L,0} = u_{V,0}$) we obtain for the mass, momentum (normal), momentum (tangential), and thermal jump conditions, respectively:

$$\dot{m} = -\rho_L v_{L,0} = \rho_V v_{V,0} \tag{18}$$

$$P_{L,0} - P_{V,0} = \dot{m}^2 \left(\frac{1}{\rho_V} - \frac{1}{\rho_L}\right) \tag{19}$$

$$-\mu_L \left(\frac{\partial v}{\partial x} + \frac{\partial u}{\partial y}\right)_{L,0} = \mu_V \left(\frac{\partial v}{\partial x} + \frac{\partial u}{\partial y}\right)_{V,0} \tag{20}$$

$$\lambda_V \left.\frac{\partial T}{\partial y}\right|_{V,0} + \lambda_L \left.\frac{\partial T}{\partial y}\right|_{L,0} = \dot{m} h_{LV} \tag{21}$$

These equations are valid for a system with two different y-coordinate directions, as shown in Fig. 1d. Next, a relation between the free-stream velocity ratio and the density ratio is found through the differentiation of (19) with respect to x, considering (18), and noting that $v_{i,0}$ (and consequently $\dot{m}$) is independent of x_i which results in

$$\left.\frac{\partial P}{\partial x}\right|_L = \left.\frac{\partial P}{\partial x}\right|_V \tag{22}$$

Finally, inserting (17) into (22) results in

$$\frac{u_{V,\infty}}{u_{L,\infty}} = \left(\frac{\rho_L}{\rho_V}\right)^{1/2} \tag{23}$$

Eqs. (18)–(21) can be re-written in non-dimensional form:

$$\frac{B_{\mathrm{p},L}}{B_{\mathrm{p},V}} = -\left(\frac{\rho_V}{\rho_L}\right)^{1/4} \left(\frac{\mu_V}{\mu_L}\right)^{1/2} \tag{24}$$

$$He_{L,0} = \frac{B_{\mathrm{p},L}^2}{2}\left(\frac{\rho_L}{\rho_V} - 1\right) + \left[\frac{u_{V,0}}{u_{V,\infty}} + \frac{\mu_V}{\mu_L}\left(1 - \frac{u_{V,0}}{u_{V,\infty}}\right)\right] \times \left(\frac{\rho_L}{\rho_V}\right)^{1/2} - 1 \tag{25}$$

$$\left(\frac{\zeta''(0)_L}{\zeta''(0)_V}\right) = -\left(\frac{\rho_L}{\rho_V}\right)^{1/4} \left(\frac{\mu_V}{\mu_L}\right)^{1/2} \tag{26}$$

$$\frac{Ja_V}{B_{\mathrm{p},V} Pr_V}\Theta_V'(0) - \frac{Ja_L}{B_{\mathrm{p},L} Pr_L}\Theta_L'(0) = 1 \tag{27}$$

Eqs. (24), (26) and (27) are equivalent to those found in [5]. The normal momentum interfacial jump condition (25), however, was not presented by the authors of [5]. This equation defines the pressure jump at the interface.

4. Problem setup and solution algorithm

We solve (12) and (13) with boundary conditions (14) for both the liquid and vapor phases, iterating to match the interfacial jump conditions (24)–(27). It should be emphasized that these equations are independent of x. We investigate the two cases of condensation of saturated and superheated vapor on subcooled liquid. A diagram of the present setup is shown in Fig. 2 for the general case including superheating of the vapor.

The procedure chosen to solve the system of equations for the case of superheated vapor on subcooled liquid is shown in Fig. 3. First, by providing the values of ρ_V/ρ_L and μ_V/μ_L and initially guessing $B_{\mathrm{p},V}$, $B_{\mathrm{p},L}$ can be calculated from (24). To prevent the possibility of cases where evaporation may occur, $B_{\mathrm{p},V}$ was restricted

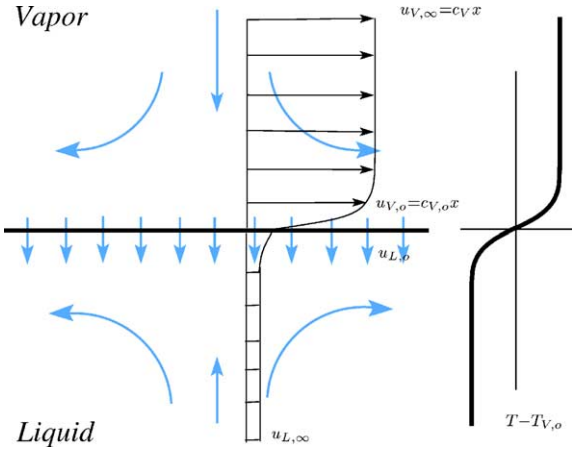

Fig. 2. Problem setup for subcooled liquid on superheated vapor.

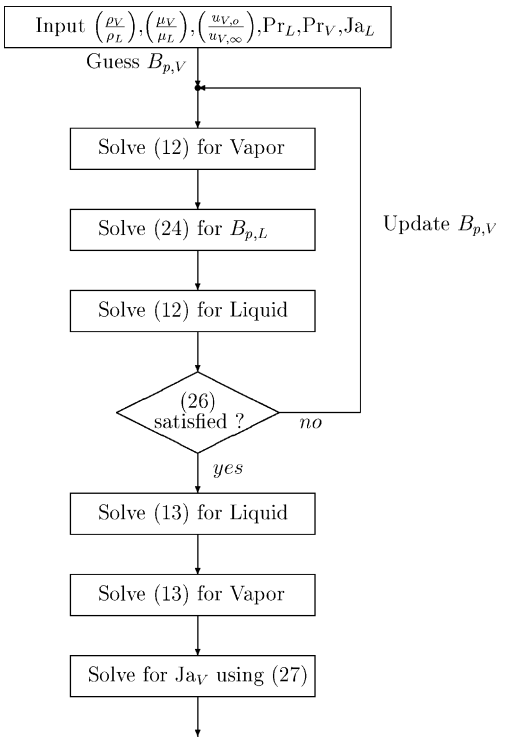

Fig. 3. Solution algorithm for superheated vapor injected into subcooled liquid.

to the range $B_{\mathrm{p},V} \leqslant 0$. Similarly, given $u_{V,0}/u_{V,\infty}$, $u_{L,0}/u_{L,\infty}$ is calculated using (23) noting that $u_{V,0} = u_{L,0}$. Knowing $B_{\mathrm{p},i}$ and $u_{i,0}/u_{i,\infty}$, the vapor and liquid momentum boundary layer equations are solved. Next, using the resultant $\zeta''(0)_i$, we check to verify whether the interface condition (26) is satisfied. If it is not within a given tolerance, $B_{\mathrm{p},V}$ is updated and the momentum boundary layer equations re-solved. Once convergence has been obtained for the velocity fields, the liquid boundary layer equation is solved to obtain $\Theta'_L(0)$ and the given Ja_L is used in (27) to obtain Ja_V. For this iterative procedure, the Bisection method was used which converges comparatively slower than other methods, but is guaranteed to converge (provided a solution exists).

The solution procedure for the case of saturated vapor on subcooled liquid differs only sightly from that described above. First, Ja_L and Pr_V are not provided as input, nor is the vapor thermal boundary layer solved. Finally, with $Ja_V = 0$ for saturated vapor, Ja_L is solved for instead of Ja_V.

The solution of the boundary layer Eqs. (12) and (13) is found using an implicit, fully second-order accurate, finite-difference solver. These equations are linearized using Picard's method and are solved with oct-precision (64 digits) via the software package "quad-double". Convergence studies on these equations were performed and dictated usage of 50,000 grid points.

4.1. Potential solution

For the case $\rho_L/\rho_V = 1$, one can obtain an analytical solution to the momentum and thermal boundary layers. Setting $\rho_L/\rho_V = 1$ in (23) one obtains $u_{V,\infty}/u_{L,\infty} = 1$. From Davis and Yadigaroglu [15] one finds that the only solution which satisfies this relation is $u_{V,0}/u_{V,\infty} = u_{L,0}/u_{L,\infty} = 1$. This is the potential solution (6) which, in non-dimensional form, becomes:

$$\zeta_i = \eta_i \tag{28}$$

$$\Theta_i = \mathrm{erf}\left[\frac{\sqrt{2}}{2} Pr_i^{1/2} \eta_i\right] \tag{29}$$

Using (28) with (26) requires that $\mu_L/\mu_V = 1$. Finally, using (28) and (29) in (24)–(27) with $\rho_L/\rho_V = 1$, $\mu_L/\mu_V = 1$, and $u_{V,0}/u_{V,\infty} = u_{L,0}/u_{L,\infty} = 1$ one obtains

$$B_{\mathrm{p},L} = -B_{\mathrm{p},V} \tag{30}$$

$$He_{L,0} = 0 \tag{31}$$

$$B_{\mathrm{p},L} = -\sqrt{\frac{2}{\pi}}\left(Ja_V Pr_V^{-1/2} + Ja_L Pr_L^{-1/2}\right) \tag{32}$$

Thus, to obtain the potential solution, one is required to provide the Jacob and Prandtl numbers for each phase. This case is of interest since any mass transfer correlations derived should reduce to this solution when $\rho_L/\rho_V = 1$, $\mu_L/\mu_V = 1$, and $u_{L,\infty}/u_{V,\infty} = 1$.

5. Case 1: Condensation of saturated vapor on subcooled liquid

For the case of saturated vapor condensing on subcooled liquid, a parametric study was performed with a total of 640 combinations of variables, with $\mu_L/\mu_V \in \{10, 20, 33.3, 40\}$, $\rho_L/\rho_V \in \{10, 100, 500, 1000\}$, $Pr_L \in \{0.5, 1, 5, 10\}$, $0.05 < u_{V,0}/u_{V,\infty} < 0.43$. Values were chosen in the range expected in water, however, it was not possible to determine, a priori, values for $u_{V,0}/u_{V,\infty}$. A parametric study was, thus, necessary to determine which combinations of these parameters would result in a solution. In addition to these variables, the potential solution (28)–(32) was also calculated for the range of Ja_L and with Pr_L given.

5.1. Results: Momentum transfer

The momentum boundary layer is found, from (14), to depend on two variables, viz., $u_{i,0}/u_{i,\infty}$ and $B_{\mathrm{p},i}$. As shown in Appendix A, the momentum boundary layer is affected more by $u_{i,0}/u_{i,\infty}$ than by $B_{\mathrm{p},i}$, for the range of interest, and the velocity ratio is thus used to describe the momentum boundary layer. The effects of varying Ja_L, ρ_L/ρ_V, and μ_L/μ_V on $u_{V,0}/u_{V,\infty}$ are shown in Fig. 4.

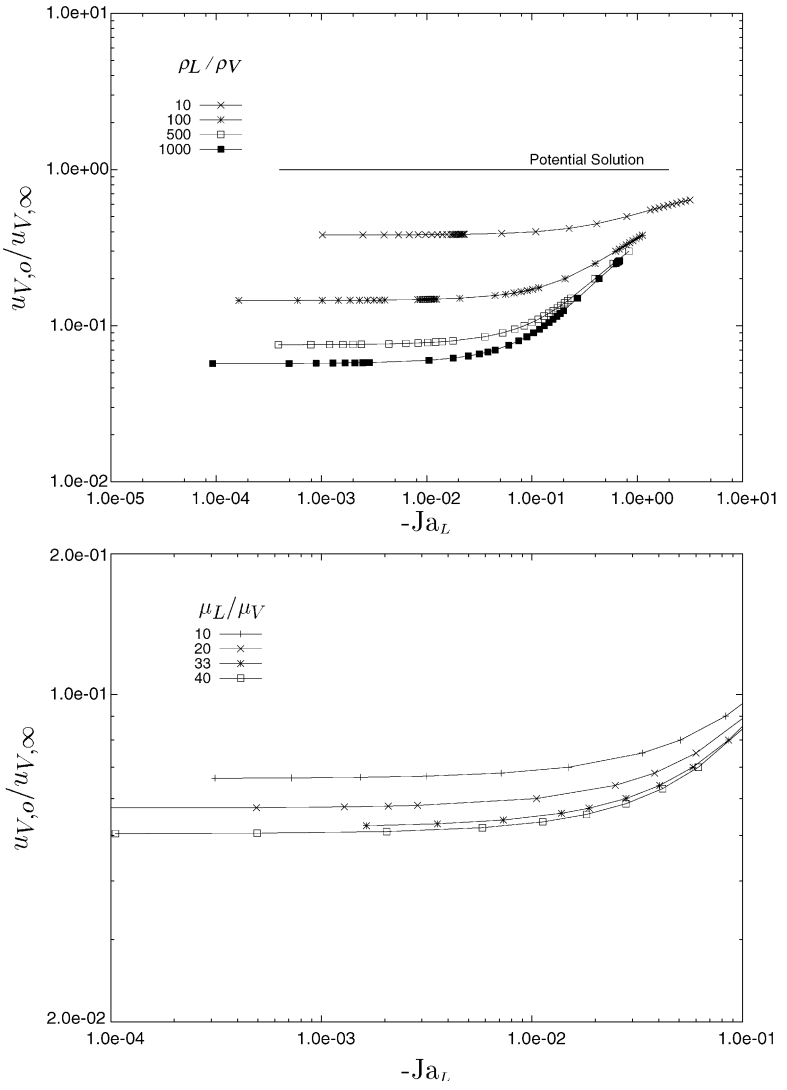

Fig. 4. (top): Effects of varying ρ_L/ρ_V and Ja_L on $u_{V,0}/u_{V,\infty}$ for $\mu_L/\mu_V = 20$ and $Pr_L = 1$ (bottom): Effects of varying μ_L/μ_V and Ja_L on $u_{V,0}/u_{V,\infty}$ for $\rho_L/\rho_V = 1000$ and $Pr_L = 1$.

First, the effect of increasing the liquid subcooling ($-Ja_L$) is shown in Fig. 4 (top). For small subcooling, one finds that $u_{V,0}/u_{V,\infty}$ is practically independant of Ja_L, suggesting that in this region the development of the momentum boundary layer is independent of the mass transfer rate that is influenced by the thermal boundary layer only. For larger subcooling ($-Ja_L > 0.01$), mass transfer increases (as shown later) and the momentum boundary layer becomes increasingly affected; the coupling between the momentum and thermal boundary layers becomes increasingly important. It is interesting to note that, as subcooling increases, $u_{V,0}/u_{V,\infty}$ approaches the potential solution (described in Section 4.1). This is, however, more of an academic exercise since for a substance such as water, for a range of 1 bar $\leqslant P \leqslant 5$ bar, $Ja_L \approx -0.15$ produces a temperature difference of approximately $\Delta T = 80$ K. Since, for practical applications involving water, $\Delta T < 100$ K, we limit our computations to $Ja_L \leqslant -0.1$ where the momentum boundary layer is found to be relatively independent of subcooling.

The effect of the density ratio ρ_L/ρ_V on the vapor momentum boundary layer is shown in Fig. 4 (top) where one finds that as ρ_L/ρ_V increases, the resulting $u_{V,0}/u_{V,\infty}$ decreases. An increase in ρ_L/ρ_V (or identically an increase in ρ_L) causes, through matching of the pressure gradients across the interface (23), a decrease in $u_{L,\infty}$ for a constant $u_{V,\infty}$. With an increase in liquid density, the tangential interfacial velocity, $u_{i,0}$, decreases; a decrease in $u_{V,0}/u_{V,\infty}$ follows.

Similar trends are shown in Fig. 4 (bottom) for the viscosity ratio where an increase in μ_L/μ_V results in a decrease in $u_{V,0}/u_{V,\infty}$. The effect of varying the viscosity ratio is, however, much smaller than that found for the density ratio (for the ranges investigated). First, an increase in μ_L/μ_V (or equivantly an increase in μ_L) does not affect the freestream velocity ratio, $u_{L,\infty}/u_{V,\infty}$, controlled by (23). Through the tangential momentum interfacial jump condition (26) and noting the variation caused in $\zeta''(0)_i$ by a change in $u_{i,0}/u_{i,\infty}$ (see Appendix A) one finds that an increase in μ_L/μ_V causes a decrease in $u_{i,0}$ and thus a decrease in $u_{i,0}/u_{i,\infty}$.

Finally, it is worth noting the effect of varying Pr_L on the momentum boundary layer. At low subcooling, Pr_L is found to have no effect on $u_{V,0}/u_{V,\infty}$, since it was already noted that the momentum boundary layer is independent of the thermal boundary layer here. Only above $-Ja_L > 0.01$ is the momentum boundary layer affected. In this region, an increase in Pr_L results in a decrease in $u_{V,0}/u_{V,\infty}$.

5.2. Results: Mass transfer

As shown by (15), the blowing parameter, $B_{\mathrm{p},i}$, which is directly related to mass transfer is used to describe the mass transfer. Since, for the present case, the vapor phase is saturated, Ja_V is identically zero and the thermal interfacial jump condition (27) becomes

$$B_{\mathrm{p},L} = -\frac{Ja_L \Theta'_L(0)}{Pr_L} \tag{33}$$

The effect of varying Ja_L, ρ_L/ρ_V, and Pr_L on $B_{\mathrm{p},L}$ is shown in Fig. 5. First, an increase in subcooling is found to result in a linear increase in mass transfer, as expected. The effect of increasing either ρ_L/ρ_V or μ_L/μ_V on mass transfer is found to be small (for the range investigated). Condensation ($B_{\mathrm{p},L}$) increases slightly with ρ_L/ρ_V as shown in Fig. 5 (top); an even smaller decrease was found for μ_L/μ_V. This trend is a result from the fact that for an increase in ρ_L/ρ_V, an increase in $u_{L,0}/u_{L,\infty}$ results and for an increase in μ_L/μ_V a small decrease in $u_{L,0}/u_{L,\infty}$ was observed. From Appendix A, this results in an increase in $\Theta'_L(0)$ with ρ_L/ρ_V and a decrease in $\Theta'_L(0)$ with μ_L/μ_V. Finally, Fig. 5 (bottom) shows the effect of varying Pr_L (equivalent to varying λ_L) on mass transfer. Here one finds that Pr_L has a much more pronounced effect than the viscosity or density ratios and results in a decrease in mass transfer with Pr_L. Since, the effects of varying Pr_L on the momentum boundary layer are shown to be relatively small, the effect of varying Pr_L comes from the thermal interfacial jump condition (33).

Although an increase in Pr_L results in an increase in $\Theta'_L(0)$ [16] (also shown in Appendix A), the inversely proportional effect of Pr_L on $B_{\mathrm{p},L}$ is stronger and $B_{\mathrm{p},L}$ decreases with Pr_L.

5.3. Correlation of the mass transfer rate

Using the results of the computations, a correlation was found for the relationship between $B_{\mathrm{p},L}$, Ja_L and the other parameters, which is independent of x, and took the form

$$B_{\mathrm{p},L} = -\sqrt{\frac{2}{\pi}}\left(\frac{\mu_L}{\mu_V}\right)^{-1/20}\left(\frac{\rho_L}{\rho_V}\right)^{1/20} Pr_L^{-1/2} Ja_L \tag{34}$$

valid for the range $1 \leqslant \rho_L/\rho_V \leqslant 1000$, $10 \leqslant \mu_L/\mu_V \leqslant 40$, $0.5 \leqslant Pr_L \leqslant 10$, and $-1.0\times10^{-1} \leqslant Ja_L \leqslant -1.0\times10^{-5}$. It should be noted that this form of the correlation reduces to the potential solution result (32) when $\rho_L/\rho_V = \mu_L/\mu_V = 1$ and $Ja_V = 0$:

$$B_{\mathrm{p},L} = -\sqrt{\frac{2}{\pi}} Pr_L^{-1/2} Ja_L \tag{35}$$

A comparison of the $B_{\mathrm{p},L}$ calculated using (34) with $B_{\mathrm{p},L}$ found as a result of the computations is shown in Fig. 6. Here, for the range of $B_{\mathrm{p},L}$ used, good agreement is found, with all values falling within an error range of $\pm 15\%$. Next, we compare our results of $B_{\mathrm{p},L}$ using (34) to results reported for the axi-symmetric, Homann flow, condensation solution of [18] for the range of Ja_L used in the present study. Results of the comparison are shown in Table 1, where good agreement is found. This agreement is not surprising since the Homann and Hiemenz momentum boundary layer profiles are similar [6]. To compare (34) with experimentally obtained mass fluxes one must first combine (15) and (18) resulting in

$$\dot{m} = -B_{\mathrm{p},L}(c_L \mu_L \rho_L)^{1/2} \tag{36}$$

No direct comparison with experiments was possible, since no values of c_L are reported in the literature.

5.4. Results: Heat transfer coefficient

Often in the literature, experimental results involving heat and mass transfer are presented in terms of a liquid-side heat transfer coefficient, α_L, defined as

$$\alpha_L \equiv \frac{\lambda_L \frac{\partial T}{\partial y}\Big|_{L,0}}{(T_{L,\infty} - T_{L,0})} \tag{37}$$

Using the similarity relations (9)–(11) and (6) this relation can be re-written in a familiar non-dimensional form:

$$Nu_L = \Theta'_L(0) Re_L^{1/2} \tag{38}$$

Inserting (27) into (38), with $Ja_V = 0$, one obtains a relationship for the non-dimensional heat transfer coefficient, $Nu/Re^{1/2}$:

$$\frac{Nu_L}{Re_L^{1/2}} = -\frac{B_{\mathrm{p},L} Pr_L}{Ja_L} \tag{39}$$

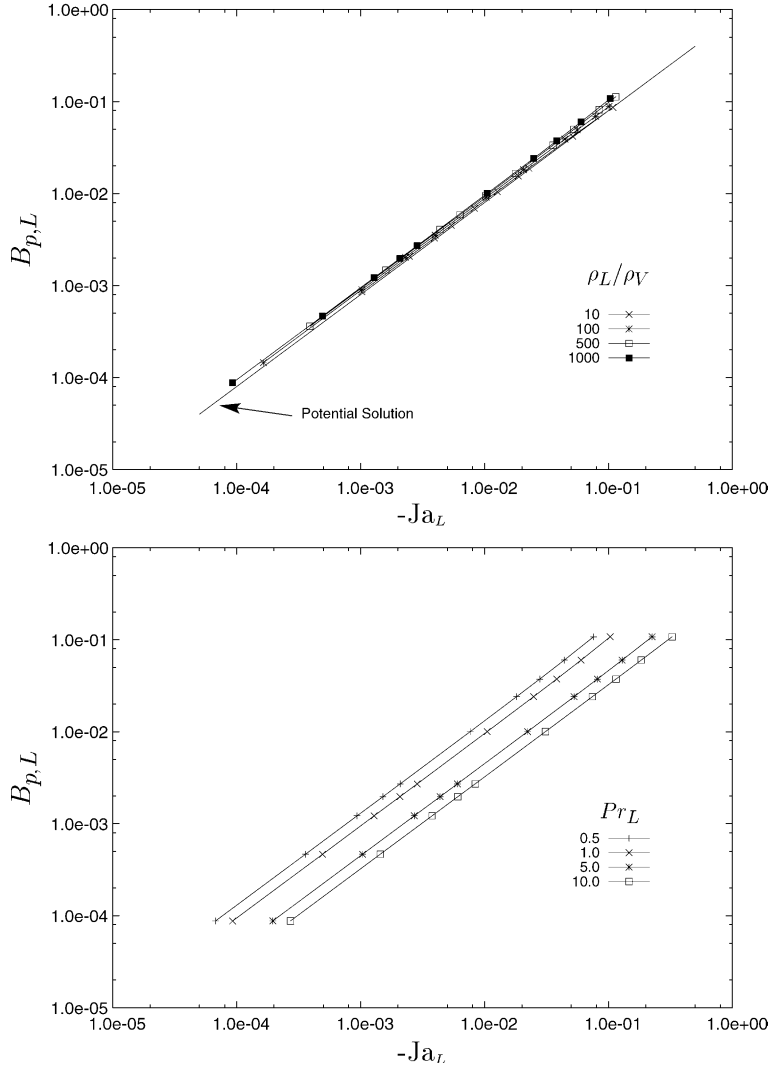

Fig. 5. (top): Effects of varying ρ_V/ρ_L and Ja_L on $B_{p,L}$ for $\mu_L/\mu_V = 20$ and $Pr_L = 1$ (bottom): Effects of varying Pr_L and Ja_L on $B_{p,L}$ for $\rho_L/\rho_V = 1000$ and $\mu_L/\mu_V = 20$.

Finally, inserting the correlation found for $B_{p,L}$ (34) into (39) one obtains a correlation for the heat transfer coefficient:

$$\frac{Nu_L}{Re_L^{1/2}} = \sqrt{\frac{2}{\pi}}\left(\frac{\mu_L}{\mu_V}\right)^{-1/20}\left(\frac{\rho_L}{\rho_V}\right)^{1/20} Pr_L^{1/2} \tag{40}$$

It is interesting to note that this relation is independent of Ja_L. Since the present study is limited to a low range of $B_{p,L}$, which, as shown in Appendix A, when varied has little effect on the momentum and thermal boundary layers, it is of interest to compare our results to those for the case $B_{p,L} = 0$. From Kays and Crawford [16] the Nusselt correlation for a Hiemenz flow with $B_{p,L} = 0$ is

$$Nu_L = 0.81 Re_L^{1/2} Pr_L^{0.4} \tag{41}$$

which is comparable to (40) in as much as both correlations show a weak dependance on viscosity.

5.5. Results: Interfacial pressure jump

An often neglected quantity is the pressure jump at the liquid–vapor interface. Noting the definition of $He_{L,0}$, which is a normalized pressure jump, a relationship can be found using (14), (16), (23), (24) and (25):

$$He_{L,0} = B_{p,L}^2\left(\frac{\rho_L}{\rho_V} - 1\right) \tag{42}$$

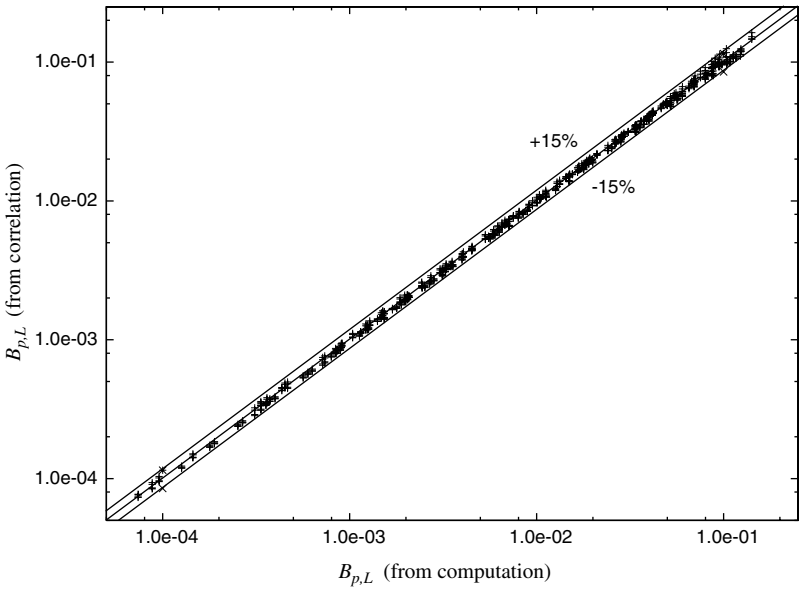

Fig. 6. Comparison of $B_{p,L}$ with estimated $B_{p,L}$ from (34).

Table 1
Comparison of $B_{p,L}$ computed from an axi-symmetric solution [18] and those computed using (34)

Ja_L	Substance	$B_{p,L}$	
		Axi-symmetric	Present study
1.91×10^{-4}	H_2O	10^{-4}	1.4×10^{-4}
1.90×10^{-3}	H_2O	10^{-3}	1.4×10^{-3}
1.85×10^{-2}	H_2O	10^{-2}	1.3×10^{-2}
3.1×10^{-2}	*R*12	10^{-2}	1.4×10^{-2}
9.2×10^{-3}	*K*	10^{-1}	1.8×10^{-1}

Using the correlation for $B_{p,L}$ (34) in (42), one obtains

$$He_{L,0}=\frac{2}{\pi}\left(\frac{\mu_L}{\mu_V}\right)^{-1/10}\left(\frac{\rho_L}{\rho_V}\right)^{1/10}Pr_L^{-1}Ja_L^2\left(\frac{\rho_L}{\rho_V}-1\right) \quad (43)$$

6. Case 2: Condensation of superheated vapor on subcooled liquid

For the case of superheated vapor condensing on subcooled liquid, a parametric study was performed with a total of 10,240 combinations of variables using $\mu_L/\mu_V \in \{10, 20, 33.3, 40\}$, $\rho_L/\rho_V \in \{10, 100, 500, 1000\}$, $Pr_L \in \{0.5, 1, 5, 10\}$, $Pr_V \in \{0.75, 1, 1.25, 1.5\}$, $-Ja_L \in \{10^{-4}, 10^{-3}, 10^{-2}, 10^{-1}\}$ and, $0.05 < u_{V,0}/u_{V,\infty} < 0.43$, chosen to correspond to values expected in water. Here, we also obtained the solution to the potential flow problem (28)–(32) for the range of Ja_V, Ja_L, Pr_L, and Pr_V.

6.1. Results: Mass transfer

As in the case of saturated vapor on subcooled liquid, we use $B_{p,L}$ as a measure of mass transfer. To include the effect of superheat, we assume that mass transfer for the case of superheated vapor, $B_{p,L,sup}$, can be described as the mass transfer found in a saturated case, $B_{p,L,sat}$, multiplied by a correction factor taking into account the effects of superheat, Φ_{sup}:

$$B_{p,L,sup}=B_{p,L,sat}\Phi_{sup} \quad (44)$$

Using (24),(27) and (33) one finds an analytical relation for Φ_{sup}:

$$\Phi_{sup}=1-\left(\frac{\rho_V}{\rho_L}\right)^{1/4}\left(\frac{\mu_V}{\mu_L}\right)^{1/2}\left(\frac{Pr_L}{Pr_V}\right)\left(\frac{-Ja_V}{Ja_L}\right)\left(\frac{\Theta'_V(0)}{\Theta'_L(0)}\right) \quad (45)$$

Using (44) and (34), the results of the present computations for Φ_{sup} for various Ja_V, Ja_L, ρ_L/ρ_V, μ_L/μ_V, Pr_L,

and Pr_V are shown in Figs. 7, 8. First, one finds that, for low superheats, the effect on mass transfer is small, as expected. As the superheat increases, the liquid becomes unable to absorb all the latent heat of the vapor and the rate of mass transfer decreases.

Next, Fig. 7 (top) shows the effect of varying ρ_L/ρ_V on Φ_{sup}. Here one finds that Φ_{sup} increases with the density ratio, lessening the negative effect of the superheat. This is readily seen in (45) where $\lim_{\rho_L/\rho_V\to\infty}\Phi_{\text{sup}} = 1$. Similar effects are found in Fig. 7 (bottom) where an increase in μ_L/μ_V results in an increase in Φ_{sup}, lessening again the effects of superheat. The effects of varying Pr_L and Pr_V on Φ_{sup} are found to have a similar effect as that of ρ_L/ρ_V. Here, however, an increase in Pr_L results in a decrease in Φ_{sup}, whereas an increase in Pr_V results in a increase in Φ_{sup}, thus enhancing the effects of superheat. Finally, the effect of varying Ja_L on Φ_{sup} is shown in Fig. 8. Here one finds that increasing the liquid subcooling results in an increase in Φ_{sup}.

To obtain a correlation for Φ_{sup}, the dimensionless interfacial temperature gradient ratio $\Theta'_V(0)/\Theta'_L(0)$ in (45) was assumed to take the form

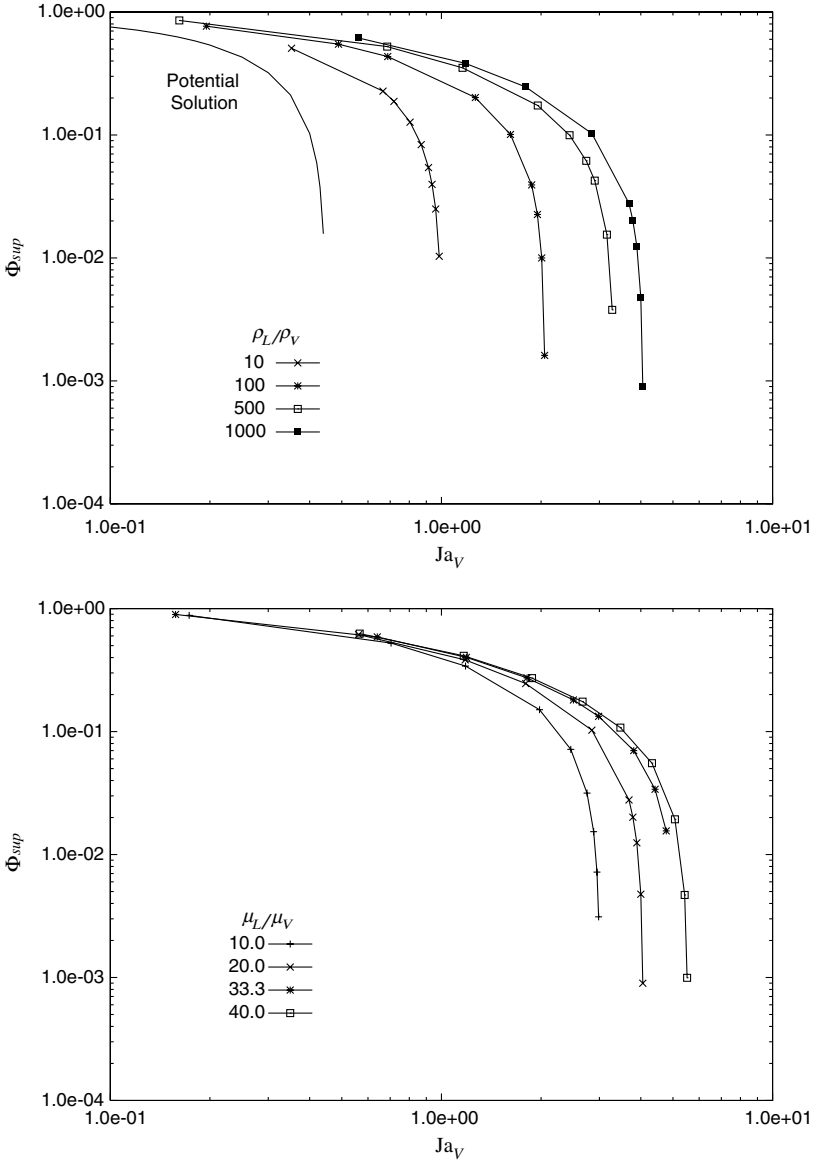

Fig. 7. (top): Effects of varying ρ_V/ρ_L and Ja_V on Φ_{sup} for $\mu_L/\mu_V = 20$, $Pr_L = 1$ $Pr_V = 1$, and $Ja_L = -0.1$ (bottom): Effects of varying μ_L/μ_V and Ja_V on Φ_{sup} for $\rho_L/\rho_V = 1000$, $Pr_L = 1$, $Pr_V = 1$, and $Ja_L = -0.1$.

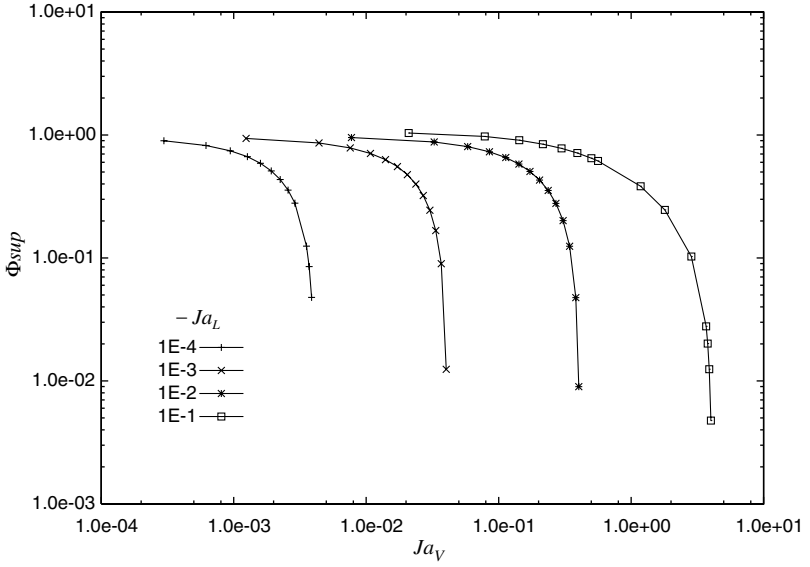

Fig. 8. Effects of varying Ja_L and Ja_V on Φ_{sup} for $\rho_L/\rho_V = 1000$, $\mu_L/\mu_V = 20$, $Pr_L = 1$, and $Pr_V = 1$.

Table 2
Coefficients for Φ_{sup} correlation in (47)

	b_1	b_2	b_3	b_4	b_5	b_6	b_7
$\Phi_{\text{sup}} < 0.1$	0.875	−0.110	−0.170	0.175	−0.220	−0.380	0.375
$0.1 \geqslant \Phi_{\text{sup}} < 0.3$	0.855	−0.098	−0.143	0.148	−0.188	−0.330	0.360
$0.3 \geqslant \Phi_{\text{sup}} < 0.6$	0.750	−0.100	−0.160	0.150	−0.190	−0.365	0.420
$\Phi_{\text{sup}} \geqslant 0.6$	0.580	−0.130	−0.145	0.165	−0.250	−0.510	0.645

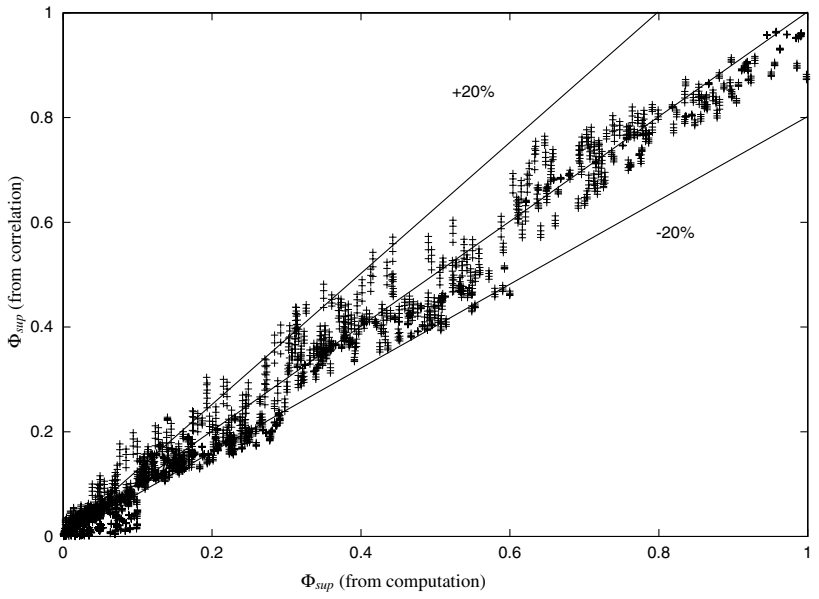

Fig. 9. Comparison of Φ_{sup} with estimated Φ_{sup} from (47).

$$\frac{\Theta'_V(0)}{\Theta'_L(0)} = a_1\left(\frac{\rho_L}{\rho_V}\right)^{a_2}\left(\frac{\mu_L}{\mu_V}\right)^{a_3} Pr_L^{a_4} Pr_V^{a_5}(-Ja_L)^{a_6} Ja_V^{a_7} \qquad (46)$$

which when replaced in (45) leaves

$$\Phi_{\text{sup}} = 1 - b_1\left(\frac{\rho_L}{\rho_V}\right)^{b_2}\left(\frac{\mu_L}{\mu_V}\right)^{b_3} Pr_L^{b_4} Pr_V^{b_5}(-Ja_L)^{b_6} Ja_V^{b_7} \qquad (47)$$

where the a_i and b_i are constant coefficients. Using (47), the results were found to fit best with the coefficients shown in Table 2, valid for the range $1 \leqslant \rho_L/\rho_V \leqslant 1000$, $10 \leqslant \mu_L/\mu_V \leqslant 40$, $0.5 \leqslant Pr_L \leqslant 10$, $0.75 \leqslant Pr_V \leqslant 1.50$, $1.1 \times 10^{-4} \leqslant Ja_V \leqslant 9.7 \times 10^{0}$, and $-1.0 \times 10^{-1} \leqslant Ja_L \leqslant -1.0 \times 10^{-4}$. Here, an iterative strategy is required to determine which coefficients to use. A comparison of the Φ_{sup} calculated using (47) with the computed Φ_{sup} values is shown in Fig. 9. The agreement is not as good as that for the saturated case. However, there is acceptable agreement for higher values of Φ_{sup} and, in general, the agreement deteriorates with decreasing Φ_{sup}. We note that the source of error in this correlation is from the assumed form of $\Theta'_V(0)/\Theta'_L(0)$. Finally, we make a comparison of the results for water. For a given saturation pressure in the range 1–5 bar and a temperature range 10–70 °K one finds [19] that the liquid and vapor Jacob numbers fall in the ranges $10^{-2} < -Ja_L < 10^{-1}$ and $10^{-2} < \text{Ja}_V < 10^{-1}$. Using (47) (and noting that variations of Pr_i, ρ_L/ρ_V, and μ_L/μ_V are secondary effects)

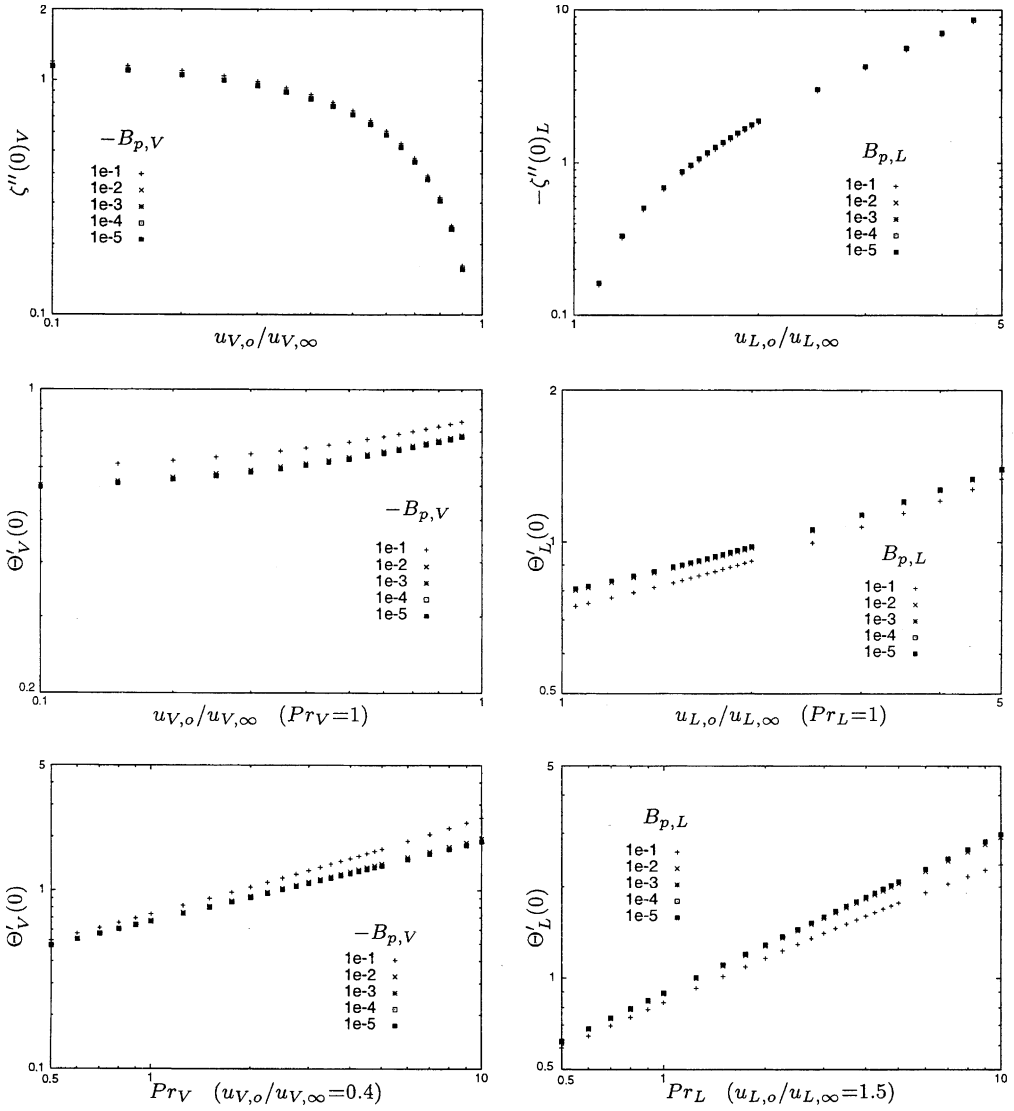

Fig. 10. Solutions to Hiemenz boundary layer equations for the vapor (left) and liquid phase (right).

one finds that $\Phi_{\text{corr}} \approx 1$. This suggests that the effects of superheat for practical applications involving water are negligible, which is in accordance with [5,12].

7. Conclusions

Parametric studies for direct contact condensation in a Hiemenz flow of saturated and superheated vapor on subcooled liquid have been performed numerically. For the case of saturated vapor we find that:

- The effects of varying ρ_L/ρ_V and μ_L/μ_V on mass transfer are small, compared to the effects of Pr_L and Ja_L.
- Enhanced mass transfer can be obtained by increasing $-\text{Ja}_L$, ρ_L/ρ_V or decreasing Pr_L, μ_L/μ_V.
- Mass transfer is represented well by (34) which can be used to define a correlation for the heat transfer coefficient (40) and compute the interfacial pressure difference (43). Results are independent of x.

For the case of superheated vapor we find that:

- Varying μ_L/μ_V, ρ_L/ρ_V, Pr_L, Pr_V, and Ja_L has little effect on Φ_{corr} for small values of the superheat, larger effects for larger values of Ja_V.
- Enhanced mass transfer can be obtained by increasing $-Ja_L$, Pr_V, ρ_L/ρ_V, μ_L/μ_V or decreasing Ja_V, Pr_L.
- Mass transfer for superheated vapor has been shown to correlate reasonably well as a correction to mass transfer in saturated vapor using (44) and (47). The results are, again, independent of x.

Appendix A. Solutions to the Hiemenz boundary layer equations

The Hiemenz flow boundary layer equations for phase i are:

$$\zeta_i''' + \zeta_i\zeta_i'' - (\zeta_i')^2 + 1 = 0 \tag{A.1}$$

$$\Theta_i'' + Pr_i\zeta_i\Theta_i' = 0 \tag{A.2}$$

with the boundary conditions

$$\eta_i \to \infty \begin{cases} \zeta_i' \to 1 \\ \Theta_i \to 1 \end{cases}, \quad \eta_i = 0 \begin{cases} \zeta_i = -B_{\text{p},i} \\ \zeta_i' = u_{i,0}/u_{i,\infty} \\ \Theta_i = 0 \end{cases} \tag{A.3}$$

The solution to these equations solved independently for both the vapor and liquid phases, for the ranges of $B_{\text{p},i}$, $u_{i,0}/u_{i,\infty}$, and Pr_i expected in the study, are shown in Fig. 10. First, for both the liquid and vapor phase one finds that $\zeta''(0)_i$ and $\Theta_i'(0)$ are relatively insensitive to $B_{\text{p},i}$ when $|B_{\text{p},i}| < 0.1$. This suggests that below this limit an increase in mass transfer will not alter significantly either the momentum or temperature boundary layers. For the momentum boundary layer, an increase in $u_{V,0}/u_{V,\infty}$ results in a decrease in $\zeta''(0)_V$ and an increase in $\Theta_V'(0)$. For the liquid phase, an increase in $u_{L,0}/u_{L,\infty}$ results in an increase in both $-\zeta''(0)_L$ and $\Theta_L'(0)$. Finally, an increase in the Prandtl number for both the liquid and vapor phase result in an increase in $\Theta_i'(0)$.

References

[1] K. Hiemenz, Die Grenzschicht an einem in den gleichförmigen Fluessigkeitsstrom eingetauchten geraden Kreiszylinder, Dinglers Polytech. J. 326 (1911) 1–311.
[2] H. Schlichting, Boundary-Layer Theory, sixth ed., McGraw-Hill, New York, 1968.
[3] C. Wang, Stagnation flow on the surface of a quiescent fluid—an exact solution of the Navier–Stokes equations, Q. Appl. Math. 43 (1985) 215–223.
[4] J. Stuart, Double boundary-layers in oscillatory viscous flow, J. Fluid Mech. 24 (1966) 673–687.
[5] F. Gerner, C. Tien, Axi-symmetric interfacial condensation model, J. Heat Transfer 111 (1989) 503–510.
[6] F. Homann, Der Einfluss grosser Zähigkeit bei der Stromung um den Zylinder und um die Kugel, Z. Angew. Math. Mech. 16 (1936) 153–164.
[7] A. Coward, P. Hall, The stability of two-phase flow over a swept wing, J. Fluid Mech. 329 (1996) 247–273.
[8] C. Boyadjiev, I. Halatchev, The linear stability in systems with intensive mass transfer-II. Gas–Liquid, Int. J. Heat Mass Transfer 39 (1996) 2581–2585.
[9] H. Blasius, Die Grenzschichten in Flussigkeiten mit kleinen Reibung, Z. Angew. Math. Phys. 56 (1908) 1–37.
[10] B. Tilley, P. Weidman, Oblique two-fluid stagnation-point flow, Eur. J. Mech. B 17 (1998) 205–217.
[11] E. Sparrow, S. Lin, Condensation heat transfer in the presence of a noncondensable gas, J. Heat Transfer 86 (1964) 430–436.
[12] W. Minkowycz, E. Sparrow, Condensation heat transfer in the presence of non-condensables, interface resistance, superheating, variable properties, and diffusion, Int. J. Heat Mass Transfer 9 (1966) 1125–1144.
[13] J. Mitrovic, Effects of vapor superheat and condensate subcooling on laminar film condensation, J. Heat Transfer 122 (2000) 192–196.
[14] T. Fujii, Theory of Laminar Film Condensation, Springer-Verlag, New York, 1991.
[15] J. Davis, G. Yadigaroglu, Direct contact condensation in Falkner–Skan flows, in: Proc. IMECE'02 Nov.17–22, New Orleans, USA (2002), paper 32056.
[16] W. Kays, M. Crawford, Convective Heat and Mass Transfer, third ed., McGraw-Hill, New York, 1993.
[17] J. Delhaye, Jump conditions and entropy sources in two-phase systems. Local instant formulation, Int. J. Multiphase Flow 74 (1974) 395–409.
[18] F. Gerner, Interfacial Convection and Conduction, PhD dissertation, University of California, Berkeley, 1988.
[19] E. Schmidt, Properties of Water and Steam in SI-Units, Springer-Verlag, Berlin, 1982.